ICAS 2021 SHANGHAI
International Council of the Aeronautical Sciences
32nd Congress of the International Council of the Aeronautical Sciences
September 6-10, 2021
Pudong Shangri-La, Shanghai, China

MODELING AND SIMULATION OF DUSTY GAS FLOW IN AERODYNAMICS

Yu.M. Tsirkunov[1], D.A. Romanyuk[1] & S.V. Panfilov[1]

[1]Baltic State Technical University, 1st Krasnoarmeiskaya str. 1, Saint Petersburg 190005, Russia

Abstract

In the present paper some problems of mathematical modeling and computational simulation of two-phase gas-particle flow, as applied to aerodynamics, are discussed, and the results relating to the dispersed phase flow structure and energy flux to the body surface are presented. The main attention is paid to modeling and simulation of random phenomena: collisions between particles, scattering of non-spherical particles from a body surface, particle size dispersion. These phenomena are typical for actual gas-particle flows, but they are not taken into account in the classical two-phase gas-particle flow theory. A kinetic model and a Direct Simulation Monte Carlo method are used for calculation of a "collisional gas" of particles in the carrier gas flow. A new three-dimensional particle-wall collision model is proposed. Scattering of non-spherical particles of different shape rebounded from a smooth solid surface is studied by direct numerical simulation of rebounding the great number of particles. The lognormal law was taken for the particle size distribution in an undisturbed flow. The developed approach is incorporated into the gas-particle flow model, and the investigation of the particle phase flow structure is carried out for high-speed gas-particle flow over a blunt body (cross-wise cylinder). The distribution of the particle energy loss in particle-wall collisions along the body contour is calculated for particles of different shape. The shielding effect of the particle-particle collisions on the energy loss is discussed.

Keywords: gas-particle flow, scattering of rebounded non-spherical particles, particle-particle collisions, particle energy loss in particle-wall collisions

1. Introduction

Scientists and engineers face the problem of two-phase aerodynamics when they study and analyze a flight of vehicle in a dusty atmosphere. The atmosphere dust loading can be caused by volcanic eruptions, dusty storms, sizable fires, etc. The key engineering problems can be formulated as follows: (1) how does the dispersed phase influence the drag force and heat transfer, and (2) what is the rate of surface erosion due to particles' impacts. As is seen, the prime and immediate interest is focused on the functionals of a two-phase gas-particle flow. Experimental and theoretical results on the subject obtained by 2007 are accumulated in [1]. Eventually these functionals are determined by the gas-particle flow structure and particle impact interaction with the streamlined surface. The carrier gas and the dispersed phase behaviour depends on micro- and macro-phenomena, like the gas-particle interaction, the particle-particle collisions, the particle-wall impact interaction, the collective effects in a gas-particle mixture, and the effect of particles on a carrier gas flow. Consideration and study of these phenomena refers to the fundamentals of the multiphase flow mechanics. Specific features of particle phase flow patterns over bodies, as well as mathematical models of some "elementary" interactions in such flows and the basic regimes of flows were analyzed in [2]. Different specific aspects of the problem were studied and analyzed later in [3]–[7]. Some of the most important results entered into the review paper [8].

As is known, the classical theory of two-phase gas-particle flow assumes that particles are equal in size, have spherical shape, do not collide with each other, and rebound regularly from a streamlined surface. In actual gas-particle flow, these assumptions are not valid. In recent time a considerable number of publications have been devoted to more realistic effects: interaction of non-spherical

particles with the carrier gas flow [9]–[12], non-spherical particle-wall collisions [13]–[16], flow of polydisperse particle phase [17]–[18]. Systematic experimental investigations on particle-wall impact interaction continue for more than thirty five years [19]–[21]. Much attention was given to development of high-speed particle-wall impact interaction models with taking account for mechanical properties of the particles and the wall [24]–[25]

In spite of considerable efforts of many researchers, many questions remain open up to now. Among them modeling of some random phenomena in high speed gas-particle flows, development of the wall abrasive erosion and forming the landscape of wall roughness. The aim of the present study is to propose a new model of high-speed particle-wall impact interaction and investigate scattering of rebounded particles, to extend a developed earlier approach for a collisional "gas" of particles [26] to taking account for particle scattering, to investigate a high-speed dusty gas flow over a blunt body by an example of cross-wise cylinder, and to estimate the energy flux from the particle phase to the body surface.

2. Three-dimensional particle-wall collision model

The particle-wall impact interaction has an essential effect on the pattern and properties of dusty gas flow. The important feature of particle-wall collisions in two-phase aerodynamics is high speed particle impacts. The majority of particle-wall collision models are based on the information about the coefficients of restitution for the velocity components [7]–[8], [19]–[21], [24], [27]. A very few papers are devoted to collision modelling with explicit inclusion of mechanical properties of a particle and a wall [22], [23], [25]. In actual flows particles are not spherical in shape (see Fig. 1), and the direction of their rebound is random. A non-spherical particle can have experienced more than one collisions with the wall during rebounding before it flies away.

Figure 1 – Shape of natural and manufactured particles.

At first we consider an isolated collision of a particle with a flat wall and then investigate statistic parameters of rebounded non-spherical particles taking account for all collisions during a process of rebound. Here we describe a new 3D particle-collision model which represent a substantial modification of the developed earlier model [14]. Let $OXYZ$ be the local Cartesian coordinate system with the XZ-plane coincident with the wall surface and the Y-axis normal to it (XZ-plane will be referred to as the plane of impact). Denote the coordinates of the particle gravity center by $X_\mathrm{p}, Y_\mathrm{p}, Z_\mathrm{p}$. We introduce also the particle-fixed coordinates $O_\mathrm{p}\xi\eta\zeta$ with the axes directed along the particle principal axes of inertia. The angles φ, ψ, ϑ define the particle orientation with respect to the coordinate system $OXYZ$ and particle shapes in the present study are shown in Fig. 2.

The 'hard particle model' [28] will be used in simulating the particle-wall collisions. Let the vectors of the particle translational and angular velocities, $\mathbf{V}_\mathrm{p}$ and $\mathbf{\Omega}_\mathrm{p}$, and the angles φ, ψ, ϑ be given just before a collision. The problem is to determine the post-collisional particle translational and angular velocities. Assume that the particle-wall collision occurs at a point which will be designated as the contact point (point C in Fig. 3). If the contact area is an edge or a face of a prismatic particle, we consider the geometric center of the edge or the face as the contact point to avoid the uncertainty in

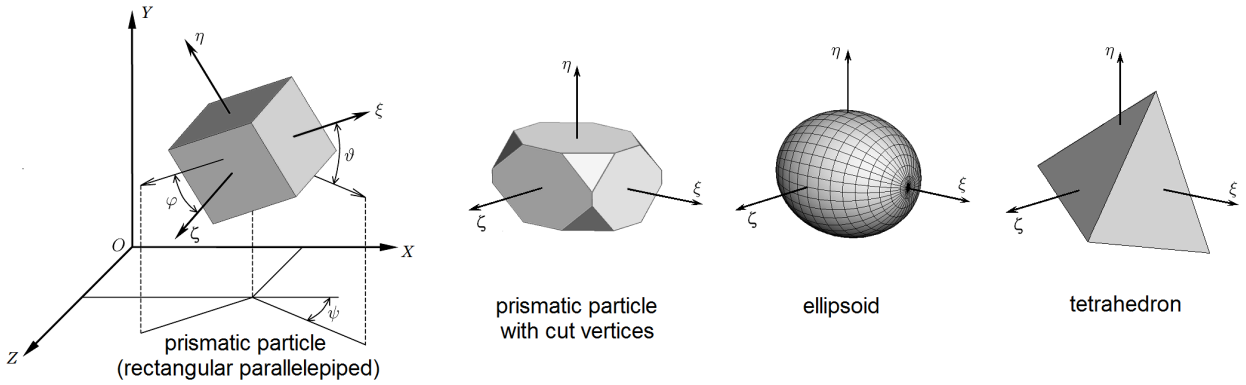

Figure 2 – Particle configuration and the angles φ, ψ, ϑ defining the particle orientation in space.

calculations. The position of the contact point with respect to the particle center of gravity is defined by the vector $\mathbf{r}_c$.

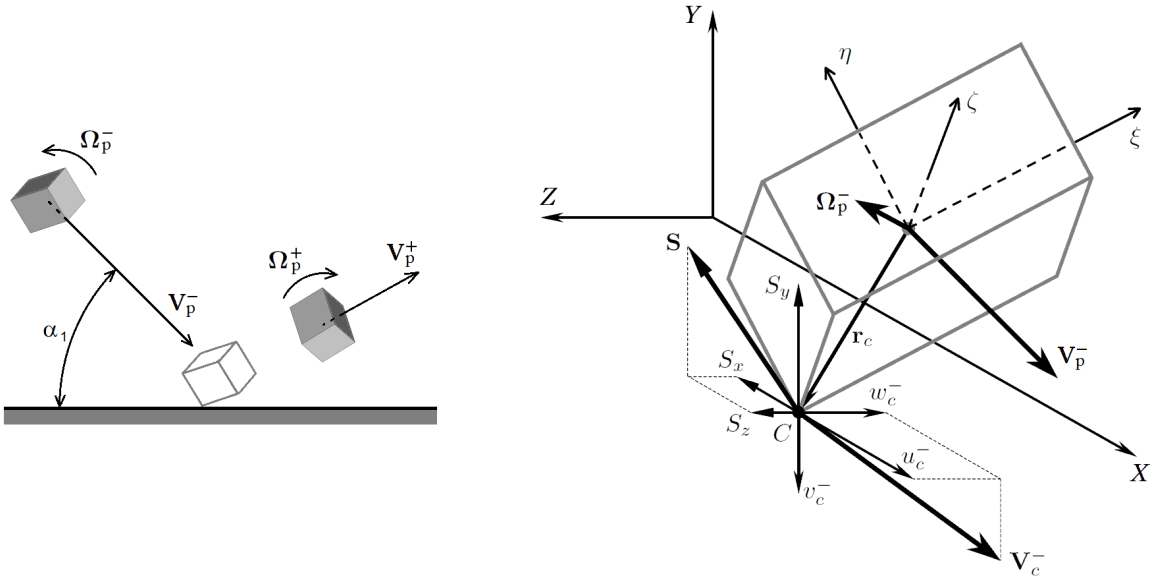

Figure 3 – Collision of a non-spherical particle with a wall.

We assume that the collision duration is very short, so that the particle position relative to the wall surface does not changes during the collision process. The equations for the change of the particle momentum and angular momentum can be written in the following integrated form

$$m_{\mathrm{p}}(\mathbf{V}_{\mathrm{p}}^{+} - \mathbf{V}_{\mathrm{p}}^{-}) \equiv m_{\mathrm{p}} \triangle \mathbf{V}_{\mathrm{p}} = \int_0^{\delta t} \mathbf{f}_c(t)\mathrm{d}t \equiv \mathbf{S}, \qquad \|J_{\mathrm{p}}\| \, (\mathbf{\Omega}_{\mathrm{p}}^{+} - \mathbf{\Omega}_{\mathrm{p}}^{-}) \equiv \|J_{\mathrm{p}}\| \triangle \mathbf{\Omega}_{\mathrm{p}} = \mathbf{r}_c \times \mathbf{S}, \tag{1}$$

where m_{p}, $\|J_{\mathrm{p}}\|$ are the mass and the inertia tensor of the particle, $\mathbf{f}_c$, $\mathbf{S}$ are the force and the impulse acting on the particle at the contact point, δt is the time interval in which the force $\mathbf{f}_c$ acts on the particle, superscripts "$-$" and "$+$" signify the pre- and post-collisional particle parameters (Fig. 3). The velocity of the particle contact point $\mathbf{V}_c$, and the particle translational and angular velocities $\mathbf{V}_{\mathrm{p}}$ and $\mathbf{\Omega}_{\mathrm{p}}$ are related by the kinematic equation

$$\mathbf{V}_c = \mathbf{V}_{\mathrm{p}} + \mathbf{\Omega}_{\mathrm{p}} \times \mathbf{r}_c. \tag{2}$$

From this we obtain

$$\triangle \mathbf{V}_c \equiv \mathbf{V}_c^{+} - \mathbf{V}_c^{-} = \triangle \mathbf{V}_{\mathrm{p}} + \triangle \mathbf{\Omega}_{\mathrm{p}} \times \mathbf{r}_c. \tag{3}$$

Combining Eqs. (1) and (3) yields

$$\frac{1}{m_{\rm p}}\|J_{\rm p}\|\,\triangle\mathbf{\Omega}_{\rm p} = \mathbf{r}_c \times \triangle\mathbf{V}_c - \mathbf{r}_c \times [\triangle\mathbf{\Omega}_{\rm p} \times \mathbf{r}_c]. \tag{4}$$

Equation (4) contains two unknown vectors $\triangle\mathbf{V}_c$ and $\triangle\mathbf{\Omega}_{\rm p}$.
Let $u_{\rm p}$, $v_{\rm p}$, $w_{\rm p}$ and u_c, v_c, w_c be the components of the vectors $\mathbf{V}_{\rm p}$ and $\mathbf{V}_c$ in the coordinats $OXYZ$, and $\triangle u_{\rm p}$, $\triangle v_{\rm p}$, $\triangle w_{\rm p}$ and $\triangle u_c$, $\triangle v_c$, $\triangle w_c$ be the components of the vectors $\triangle\mathbf{V}_{\rm p}$ and $\triangle\mathbf{V}_c$, respectively.
The most difficult problem in modeling the particle-wall impact interaction is in describing the force acting on a particle at the contact point C (or in the contact area in general case). Preliminary detailed simulation of the impact of a hard non-spherical particle on a ductile wall by methods of solid mechanics showed that a particle is sliding during interaction, and the post-collisional particle parameters (translational and angular velocity) depend substantially on the particle space orientation before an impact. Based on these results the following assumptions for a particle-wall collision model were taken in the present study:
(i) the tangential to the wall impulse of the force acting on a particle is proportional to the normal impulse and the mean tangential velocity of the contact point;
(ii) the restitution coefficient for the normal velocity of the particle center of gravity obtained experimentally by measuring the force acting from the particle phase on a solid plate can be applied to the normal velocity of the contact point.
In the case of low speed of particle impact the tangential impulse is usually considered to be proportional to the normal one only. However at high speed particle impact on the wall of ductile metal (namely this case is considered in the present study), the wall experiences the plastic deformation which depends on the strain velocity. The first assumption implies that this dependence is linear.
In line with these assumptions we can write

$$\begin{aligned}
\triangle u_{\rm p} &= -C_f \triangle v_{\rm p}(u_c^- + 0.5\triangle u_c)/|\mathbf{V}_c^-|,\\
\triangle w_{\rm p} &= -C_f \triangle v_{\rm p}(w_c^- + 0.5\triangle w_c)/|\mathbf{V}_c^-|,\\
\triangle v_c &= -v_c^-(a_n + 1),
\end{aligned} \tag{5}$$

The coefficient C_f in these equations may be interpreted as the coefficient of dynamic resistance to particle sliding in the tangential direction. It depends on the position of the contact point relative to the particle center of gravity at the impact instant. In the present study the following relation was taken for C_f

$$C_f = \exp[(\mathbf{r}_c \cdot \mathbf{V}_{\rm p}^-)/|\mathbf{r}_c||\mathbf{V}_{\rm p}^-|]$$

It is important to notice that the parameter a_n is the coefficient of restitution of the normal velocity of the particle gravity center, it is defined as follows $a_n = -v_{\rm p}^+/v_{\rm p}^-$, and in the present study we used for it the following experimental formula [20] which was obtained by measuring the force acting from the particle phase on a plate at different angles of impact:

$$a_n = 1 - [1 - \exp(-0.1|\mathbf{V}_c^-|^{-0.61})](v_c^-/|\mathbf{V}_c^-|).$$

The set of equations Eqs. (3)–(5 is closed. It is not linear and can be solved numerically by the method of successive iterations to give the components of vectors $\triangle\mathbf{\Omega}_{\rm p}$, $\triangle\mathbf{V}_c$ and $\triangle\mathbf{V}_{\rm p}$.
For validation of the proposed impact model, we took a mixture of particles of different shape (see Fig. 2) in equal parts. Let dimensions of particles in the directions of principal axes be $L_\xi = 2a$, $L_\eta = 2b$ and $L_\zeta = 2c$. The value of L_ξ for particles of the same shape were fixed, but ratios b/a and c/b were considered as independent random variables from the range [0.5, 1] and distributed by the normal law with mean value of 0.8 and standard deviation of 0.04. Such mixture in some sense is close to that used in experiments. Direct numerical simulation of a great number of particles ($\sim 10^8$) from this mixture was carried out using the proposed impact model to determine the particle translational and angular velocities. Every time the particle orientation was taken as random. The distributions of the rebounded particles' velocity at different impact angles, were obtained. The mean velocities and the most probability velocities were found at different impact angles.

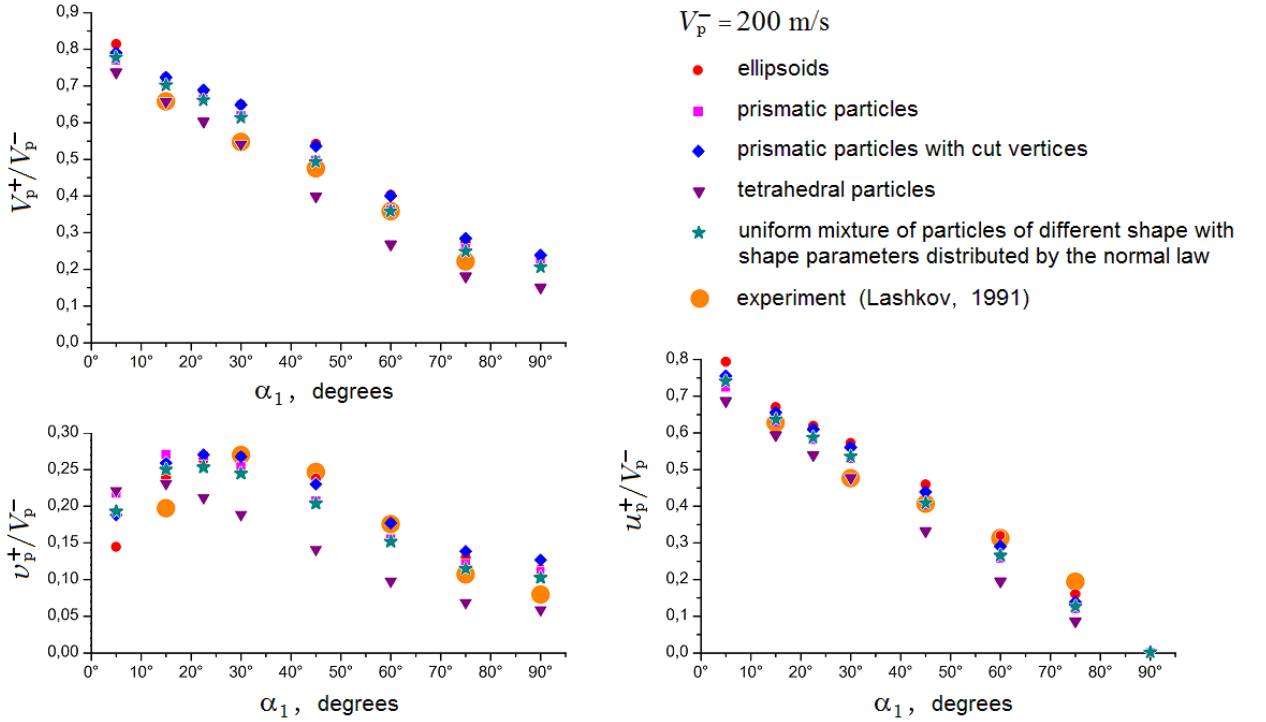

Figure 4 – Mean restitution coefficients V_p^+/V_p^-, v_p^+/V_p^- and u_p^+/V_p^- as functions of the angle of incidence α_1 for separate particle shapes and for the uniform mixture of particles of different shapes.

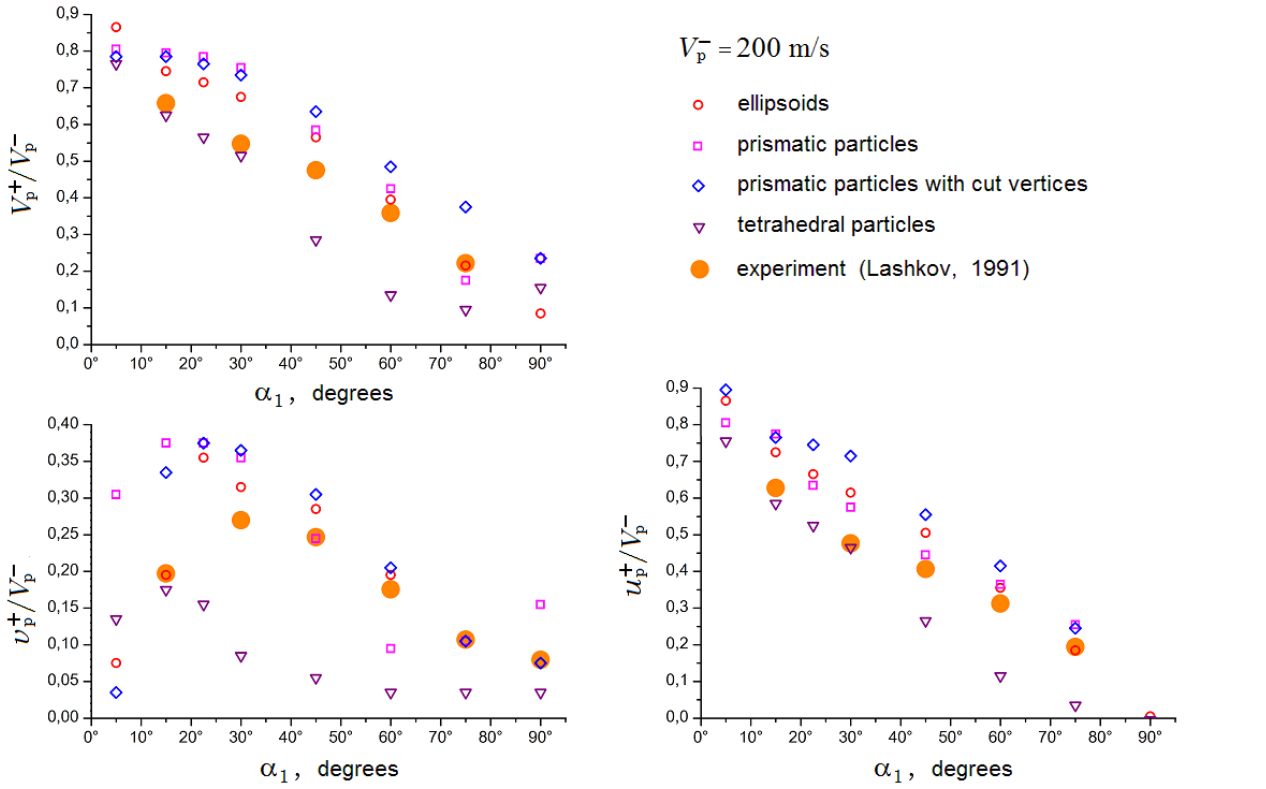

Figure 5 – Most probability ratios V_p^+/V_p^-, v_p^+/V_p^- and u_p^+/V_p^- as functions of the angle of incidence α_1 for separate particle shapes.

For comparison, the same simulations were performed for separate particle shape also with varying ratios b/a and c/b as described above. The results for the mean and most probable values of rebounded particles' velocities are shown in Figs. 4 and 5. Experimental data for mean velocities are given in these figures. It is seen that the mean and most probable velocities for every impact angle

differ noticeably from each other. The calculated results for mean velocities of particles in the mixture are on the whole in better agreement with the experimental data than those for separate particle shapes.

3. Scattering of rebounded particles

Non-spherical particles impinging on a wall at a given angle of incidence α_1 (see Fig. 3) and with the same translational and rotational velocities, $\mathbf{V}_\mathrm{p}^-$ and $\mathbf{\Omega}_\mathrm{p}^-$, rebound in different directions. Such a phenomenon is referred to as the particle scattering. It is caused by the random orientation of particles in space before the first collision. A particle can experience several collisions during one rebound. We use the particle-wall collision model described in the previous Section for each collision. Let (XY) in Fig. 6 be the plane of impact (the plane in which vector $\mathbf{V}_\mathrm{p}^-$ and the normal to the wall surface lie). The direction of the particle rebound can be defined by two angles α_2 and β_2 (Fig. 6). The angle α_2 lies in the range from 0 to π, and the angle β_2 from $-\pi/2$ to $\pi/2$.

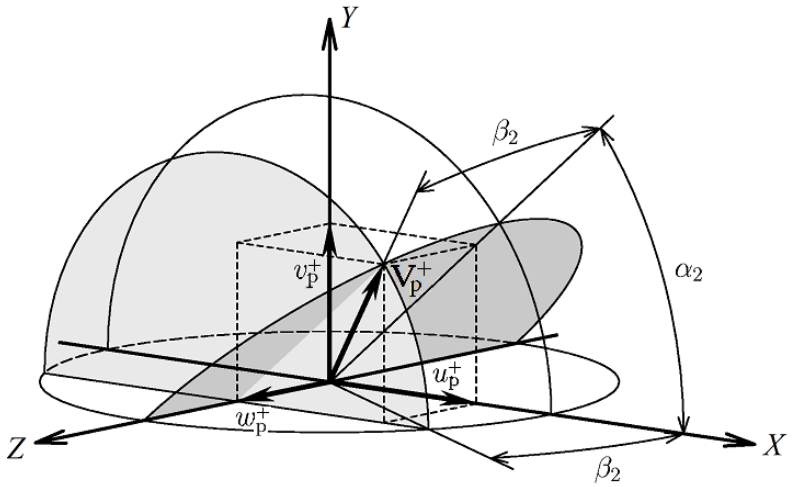

Figure 6 – Angles α_2 and β_2 define the direction of a particle rebound.

Let N be a number of incident particles with the fixed $\mathbf{V}_{\mathrm{p}1}$, $\mathbf{\Omega}_{\mathrm{p}1}$ and α_1, and $dN(\alpha_2,\beta_2,d\alpha_2,d\beta_2)$ be a number of those particles, which are reflected in the direction specified by the intervals of angles $[\alpha_2,\alpha_2+d\alpha_2]$ and $[\beta_2,\beta_2+d\beta_2]$. Introduce the distribution function $I(\alpha_2,\beta_2)$ of rebounded particles over the angles α_2 and β_2 by the relationship $I(\alpha_2,\beta_2)\,d\alpha_2\,d\beta_2 = dN(\alpha_2,\beta_2,d\alpha_2,d\beta_2)/N$. This expression represents the probability of particle rebound in the direction defined by the angles (α_2,β_2) within the intervals $d\alpha_2$ and $d\beta_2$, respectively. The function $I(\alpha_2,\beta_2)$ will be referred to as the three-dimensional (3D) scattering indicatrix. Integrating $I(\alpha_2,\beta_2)$ over β_2 from $-\pi/2$ to $\pi/2$ we obtain the two-dimensional (2D) scattering indicatrix which describes the distribution of rebounded particles over the angle α_2 (denote it by $F(\alpha_2)$).

The scattering indicatrices for particles rebounded from a smooth solid wall were calculated using the direct statistical simulation technique. In the domain of angles $0 \leqslant \alpha_2 \leqslant \pi$ and $-\pi/2 \leqslant \beta_2 \leqslant \pi/2$, we introduced the uniform rectangular grid with the steps $\triangle\alpha_2 = \triangle\beta_2 = \pi/180$ $(= 1^\circ)$. The rebound of a great number of particles ($\approx 5\cdot 10^7$) was simulated for initially non-rotating particles ($\mathbf{\Omega}_\mathrm{p}^- = 0$) at fixed ($\mathbf{V}_\mathrm{p}^-$ and α_1).

In calculations, the particle shape parameters were taken as in the previous Section. Note that the size $L_\xi = 2a$ had no effect on the indicatrices. Initial space orientation of a particle in every trial was considered as random and equiprobable. The collision model described above was used for every collision of a test particle during its rebound. For (ij)-cell of the grid, the value N_{ij} was determined as a number of particles with rebound angles α_2 and β_2 lying in the intervals $(i-1)\triangle\alpha_2 \leqslant \alpha_2 < i\triangle\alpha_2$, $(j-1)\triangle\beta_2 \leqslant \beta_2 < j\triangle\beta_2$. For large enough N, the ratio N_{ij}/N is close to the probability of reflection of a particle in the direction defined by the above indicated intervals of the angles. Then an approximate

value of the function I in the cell (ij) is calculated by the formula:

$$I(\alpha_2,\beta_2)_{ij} \approx \frac{N_{ij}}{N\Delta\alpha_2\Delta\beta_2\cos[\Delta\alpha_2(i+1/2)]}.$$

Once values of $I(\alpha_2,\beta_2)_{ij}$ are calculated in all grid cells, the distribution function $I(\alpha_2,\beta_2)$ in the whole calculation domain can be constructed. Two-dimensional (2D) scattering indicatrix $F(\alpha_2)$ in the plane XY) can be found from the relation:

$$F(\alpha_2)_i \approx \frac{\sum\limits_j N_{ij}}{N\Delta\alpha_2},$$

where the summation is over all cells (ij) with the fixed index i. A number of particles in calculations for every impact angle α_1 was about 10^8 that guaranteed statistical convergence with high accuracy. 2D indicatrices for a particle mixture described in Section 2 at different impact angles are shown in Fig. 7.

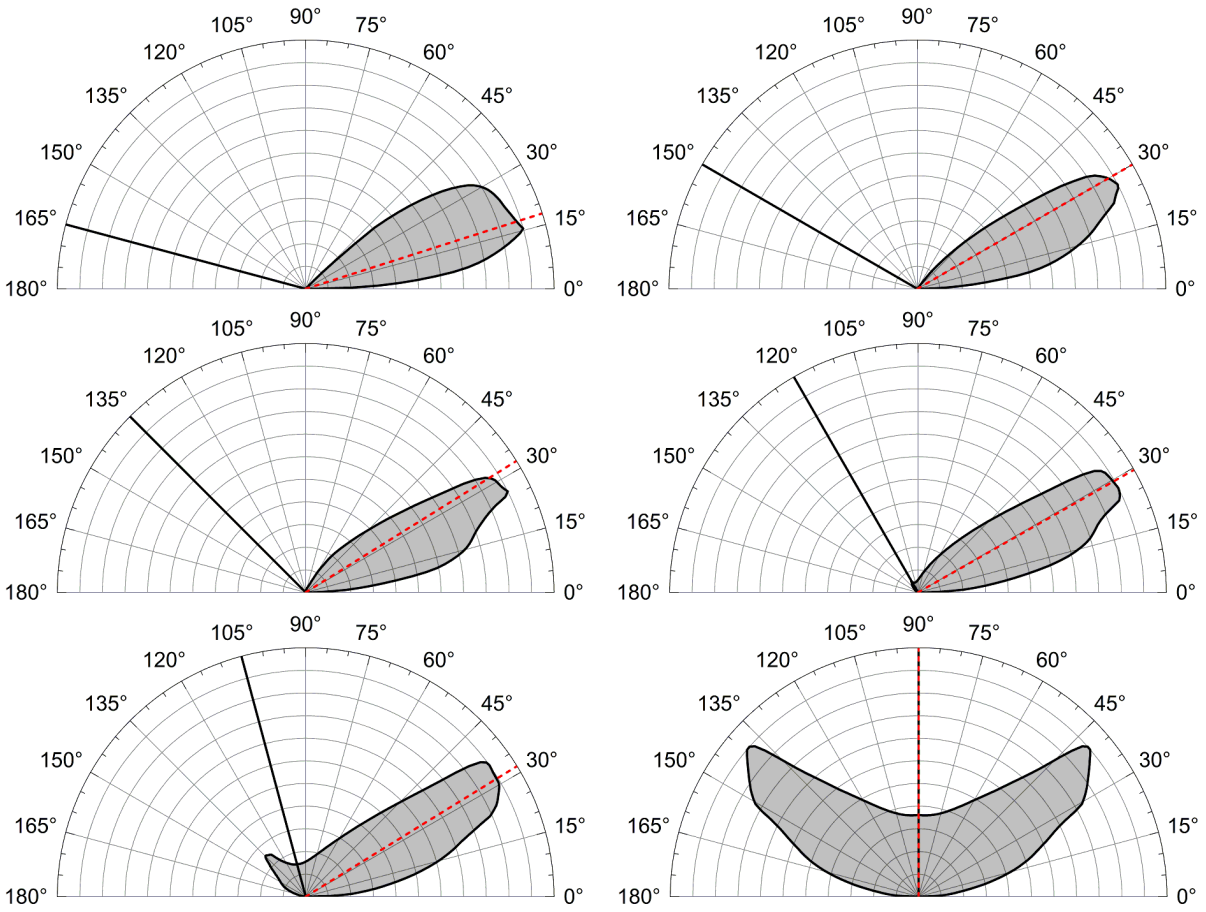

Figure 7 – 2D scattering indicatrices of rebounded particles in the plane of impact (XY). Direction of incident particles' motion is shown by solid black line; direction of spherical particles' rebound is shown by red dotted lines.

Figure 7 indicates that rebounded particles are scattered substantially at all impact angles. The most strong scattering occurs at a right impact angle. An indicatrix being one-modal in a range of impact angles $0 \leqslant \alpha_1 \lesssim 70^\circ$, becomes bemodal at angles $\alpha_1 \gtrsim 70^\circ$. Note that non-spherical particles experience not one but several collisions during the process of rebounding before it flies away from the wall.

4. Model of gas-particle interaction

The force $\mathbf{f}_\mathrm{p}$ acting on a particle includes the drag force $\mathbf{f}_\mathrm{D}$ and the lift Magnus force $\mathbf{f}_\mathrm{M}$ ($\mathbf{f}_\mathrm{p} = \mathbf{f}_\mathrm{D} + \mathbf{f}_\mathrm{M}$) which dominate over all other force components in the flow under consideration. These forces and

the torque $\mathbf{l}_\mathrm{p}$ can be expressed in terms of the dimensionless coefficients C_D, C_ω, and C_l:

$$\mathbf{f}_\mathrm{D}=\frac{1}{2}C_\mathrm{D}\pi r_\mathrm{p}^2\rho|\mathbf{v}-\mathbf{v}_\mathrm{p}|(\mathbf{v}-\mathbf{v}_\mathrm{p}),\quad \mathbf{f}_\mathrm{M}=\frac{4}{3}C_\omega\pi r_\mathrm{p}^3\rho[(\mathbf{\Omega}-\mathbf{\Omega}_\mathrm{p})\times(\mathbf{v}-\mathbf{v}_\mathrm{p})],\quad \mathbf{l}_\mathrm{p}=\frac{1}{2}C_l r_\mathrm{p}^5\rho|\mathbf{\Omega}-\mathbf{\Omega}_\mathrm{p}|(\mathbf{\Omega}-\mathbf{\Omega}_\mathrm{p}),\ (6)$$

where $\mathbf{\Omega}=(1/2)\mathrm{curl}\,\mathbf{v}$.
Although we consider particles of non-spherical shape, the model of gas-particle interaction is based on the results for spherical particles. It is partially substantiated by the closeness of drag coefficients for non-rotational spherical and non-spherical isometric particles in a wide range of Reynolds number (up to $\mathrm{Re}\sim 10^3$) [10]. The influence of particle rotation on the drag and lift forces, was studied in [11] where it was shown that the particle shape can effect on these forces. However, at present there are no suitable formulas for the drag and lift forces for non-spherical particles. Because of this we use for coefficients of the drag and lift Magnus forces, and also for the torque, correlations proposed for spherical particles. These correlations approximate the analytical, experimental and numerical data in wide ranges of the governing parameters of the flow around a single particle.
The drag coefficient C_D was calculated from the approximation formula proposed in [29]:

$$C_\mathrm{D}(\mathrm{Re}_\mathrm{p},\mathrm{M}_\mathrm{p},T_\mathrm{p}/T)=\begin{cases} C_\mathrm{D}^1, & 0<\ \mathrm{M}_\mathrm{p}\le 1,\\ C_{\mathrm{D}1}^1+\dfrac{4}{3}(\mathrm{M}_\mathrm{p}-1)(C_{\mathrm{D}2}^2-C_{\mathrm{D}1}^1), & 1<\ \mathrm{M}_\mathrm{p}\le 1.75,\\ C_\mathrm{D}^2, & \mathrm{M}_\mathrm{p}>1.75,\end{cases}\quad (7)$$

where

$$C_\mathrm{D}^1(\mathrm{Re}_\mathrm{p},\mathrm{M}_\mathrm{p},T_\mathrm{p}/T)=24\left\{\mathrm{Re}_\mathrm{p}+\sqrt{\frac{\gamma}{2}}\mathrm{M}_\mathrm{p}\left[4.33+\frac{3.65-1.53T_\mathrm{p}/T}{1+0.353T_\mathrm{p}/T}\exp\left(-0.247\sqrt{\frac{2}{\gamma}}\frac{\mathrm{Re}_\mathrm{p}}{\mathrm{M}_\mathrm{p}}\right)\right]\right\}^{-1}$$

$$+\left[\frac{4.5+0.38(0.03\mathrm{Re}_\mathrm{p}+0.48\sqrt{\mathrm{Re}_\mathrm{p}})}{1+0.03\mathrm{Re}_\mathrm{p}+0.48\sqrt{\mathrm{Re}_\mathrm{p}}}+0.1\mathrm{M}_\mathrm{p}^2+0.2\mathrm{M}_\mathrm{p}^8\right]\exp\left(-\frac{\mathrm{M}_\mathrm{p}}{2\sqrt{\mathrm{Re}_\mathrm{p}}}\right)+0.6\sqrt{\frac{\gamma}{2}}\mathrm{M}_\mathrm{p}\left[1-\exp\left(-\frac{\mathrm{M}_\mathrm{p}}{\mathrm{Re}_\mathrm{p}}\right)\right],$$

$$C_\mathrm{D}^2(\mathrm{Re}_\mathrm{p},\mathrm{M}_\mathrm{p},T_\mathrm{p}/T)=\left[0.9+\frac{0.34}{\mathrm{M}_\mathrm{p}^2}+1.86\sqrt{\frac{\mathrm{M}_\mathrm{p}}{\mathrm{Re}_\mathrm{p}}}\left(2+\frac{8}{\gamma\mathrm{M}_\mathrm{p}^2}+\frac{2.116}{\gamma\mathrm{M}_\mathrm{p}}\sqrt{\frac{T_\mathrm{p}}{T}}-\frac{4}{\gamma^2\mathrm{M}_\mathrm{p}^4}\right)\right]\cdot\left(1+1.86\sqrt{\frac{\mathrm{M}_\mathrm{p}}{\mathrm{Re}_\mathrm{p}}}\right)^{-1}.$$

Here $\mathrm{Re}_\mathrm{p}=2\rho|\mathbf{v}-\mathbf{v}_\mathrm{p}|r_\mathrm{p}/\mu$ and $\mathrm{M}_\mathrm{p}=|\mathbf{v}-\mathbf{v}_\mathrm{p}|/\sqrt{\gamma\Re T}$ are the relative particle Reynolds and Mach numbers, $C_{\mathrm{D}1}^1$ is the value of C_D^1 at $\mathrm{M}_\mathrm{p}=1$, and $C_{\mathrm{D}2}^2$ is the value of C_D^2 at $\mathrm{M}_\mathrm{p}=1.75$. The dependence of C_D on T_p/T is very week in the flow under consideration. That is why we have ignored this dependence and put $T_\mathrm{p}/T=1$.
For calculation of C_ω, the exact solution from [30] and the formula proposed in [31] were used

$$C_\omega=\begin{cases} 3/4, & 2\gamma_\omega<0.45,\\ 3/8\ \hat{C}_\omega, & 2\gamma_\omega\ge 0.45,\end{cases}\quad (8)$$

where $\gamma_\omega=|\mathbf{\Omega}-\mathbf{\Omega}_\mathrm{p}|r_\mathrm{p}/|\mathbf{v}-\mathbf{v}_\mathrm{p}|$, $\hat{C}_\omega(\gamma_\omega,\mathrm{Re}_\mathrm{p})=\gamma_\omega^{-1}[0.45+(2\gamma_\omega-0.45)\exp(-0.075\gamma_\omega^{0.4}\mathrm{Re}_\mathrm{p}^{0.7})]$.
The expression for the coefficient C_l was taken in the form proposed in [32]

$$C_l=\frac{C_{l1}}{\sqrt{\mathrm{Re}_{\mathrm{p}\omega}}}+\frac{C_{l2}}{\mathrm{Re}_{\mathrm{p}\omega}},\quad (9)$$

where $\mathrm{Re}_{\mathrm{p}\omega}=\rho|\mathbf{\Omega}-\mathbf{\Omega}_\mathrm{p}|r_\mathrm{p}^2/\mu$, and constants C_{l1} and C_{l2} are given in the Table 1.

5. Model of particle-phase motion with particle-particle collisions in gas-particle flow

Particles are more inertial than the carrier gas, and they do not follow the streamlines. Motion of particles in the flow over a body is governed by the gas-particle interaction, inter-particle collisions and impact interaction of particles with the body surface. Solid particles colliding the body rebound from it and then they can collide with the incident ones. These collisions, being random in nature, result in

Table 1 – Coefficients C_{l1} and C_{l2} in different ranges of the particle rotational Reynolds number $\mathrm{Re}_{\mathrm{p}\omega}$

$\mathrm{Re}_{\mathrm{p}\omega}$	C_{l1}	C_{l2}
$0-6$	0	16π
$6-20$	5.32	37.2
$20-50$	6.44	32.2
$50-4\cdot10^4$	6.45	32.1

chaotic motion of particles. In this Section we describe briefly a kinetic model for the collisional "gas" of dispersed particles proposed in [26].

As well as in the model of gas-particle interaction, particles in collisions between them are assumed to be hard spheres. They interact with each other only through binary collisions that is valid if the "gas" of particles is not too dense. Besides, it is assumed that collision process is instantaneous and the position of colliding particles does not change during a collision. We also consider the particles of the same radius r_{p}. The state of the i-th particle is determined by a point $\mathbf{x}_i$ of the phase space which includes the particle position vector $\mathbf{r}_i$, the particle translational and rotational velocities ($\mathbf{v}_{\mathrm{p}i}$ and $\mathbf{\Omega}_{\mathrm{p}i}$, respectively), i.e. $\mathbf{x}_i = (\mathbf{r}_i, \mathbf{v}_{\mathrm{p}i}, \mathbf{\Omega}_{\mathrm{p}i})$. The vector $\mathbf{x}_i$ is split into $\mathbf{r}_i$ and $\mathbf{y}_i = (\mathbf{v}_{\mathrm{p}i}, \mathbf{\Omega}_{\mathrm{p}i})$. We denote the parameters of the i-th and j-th particles before and after their collision by the superscripts "$-$" and "$+$", respectively. The post-collisional parameters of colliding particles are fully determined by the pre-collisional ones and the relative position of particles at the collision instant, thus we can write $\mathbf{y}_k^+ = \mathbf{y}_k^+(\mathbf{y}_i^-, \mathbf{y}_j^-, \mathbf{n}_{ij})$, $k = i, j$, where $\mathbf{n}_{ij}$ is the unit vector directed from the centre of i-th particle towards the centre of j-th particle at the instant of collision. The above relation for $\mathbf{y}_k^+$ is presumed to give a one-to-one correspondence between $\mathbf{y}_k^-$ and $\mathbf{y}_k^+$, so that the Jacobian $J_1 = |D(\mathbf{y}_i^+, \mathbf{y}_j^+)/D(\mathbf{y}_i^-, \mathbf{y}_j^-)| \neq 0$ and, hence, the relation can be resolved for the particle parameters before a collision $\mathbf{y}_k^- = \mathbf{y}_k^-(\mathbf{y}_i^+, \mathbf{y}_j^+, \mathbf{n}_{ij})$, $k = i, j$. A collision is physically feasible only when $\mathbf{g}_{ij}^- \cdot \mathbf{n}_{ij} \leq 0$, where $\mathbf{g}_{ij} = \mathbf{v}_j - \mathbf{v}_i$. We assume also that states of any two particles in the phase space are not statistically correlated. This assumption is valid if the mean free path of particles moving in the carrier gas is much smaller than the particle momentum response length. These assumptions and reasoning are similar to those accepted in rarefied gas dynamics for collisions between molecules.

Let $f_1 = f(\mathbf{x}_1, t)$ be the distribution function such that $f_1\, d\mathbf{x}_1 = f(\mathbf{r}_1, \mathbf{v}_{\mathrm{p}1}, \mathbf{\Omega}_{\mathrm{p}1}, t) d\mathbf{r}_1 d\mathbf{v}_{\mathrm{p}1} d\mathbf{\Omega}_{\mathrm{p}1}$ is the number of particles with coordinates and velocities from the elementary volume $d\mathbf{r}_1\ d\mathbf{v}_{\mathrm{p}1}\ d\mathbf{\Omega}_{\mathrm{p}1}$ in the vicinity of the point $\mathbf{x}_1 = (\mathbf{r}_1, \mathbf{v}_{\mathrm{p}1}, \mathbf{\Omega}_{\mathrm{p}1})$ of the phase space. Then, the following kinetic Boltzmann-type equation for f_1 can be derived

$$\frac{\partial f_1}{\partial t} + \frac{\partial}{\partial \mathbf{r}_1}(\mathbf{v}_{\mathrm{p}1} f_1) + \frac{\partial}{\partial \mathbf{v}_{\mathrm{p}1}}\left(\frac{\mathbf{f}_{\mathrm{p}1}}{m_{\mathrm{p}}} f_1\right) + \frac{\partial}{\partial \mathbf{\Omega}_{\mathrm{p}1}}\left(\frac{\mathbf{l}_{\mathrm{p}1}}{I_{\mathrm{p}}} f_1\right) = I_{\mathrm{coll}}\ . \tag{10}$$

This equation is a particular case of the more general kinetic equation [26] which also takes gas-particle heat transfer and particle size distribution into account. The collisional integral in the right-hand side is given by

$$I_{\mathrm{coll}} = 4 r_{\mathrm{p}}^2 \int d\mathbf{y}_2 \int\limits_{\mathbf{g}_{12}\cdot\mathbf{n}_{12}\leq 0} \left(\frac{f_1^- f_2^-}{J} - f_1 f_2\right) |\mathbf{g}_{12}\cdot\mathbf{n}_{12}| \sin\chi_{12} d\chi_{12} d\varepsilon_{12}, \qquad J = \left|\frac{\mathbf{g}_{12}\cdot\mathbf{n}_{12}}{\mathbf{g}_{12}^-\cdot\mathbf{n}_{12}} J_1\right|. \tag{11}$$

Here m_{p} and I_{p} are the particle mass and moment of inertia, $\mathbf{f}_{\mathrm{p}1}$ and $\mathbf{l}_{\mathrm{p}1}$ are the force and the torque acting on a particle from the carrier gas which are calculated for the particle with the parameters $(\mathbf{v}_{\mathrm{p}1}, \mathbf{\Omega}_{\mathrm{p}1})$ at the point $\mathbf{r}_1$ of flow, $f_2 = f(\mathbf{r}_1, \mathbf{y}_2, t)$, $f_1^- = f(\mathbf{r}_1, \mathbf{y}_1^-, t)$, $f_2^- = f(\mathbf{r}_1, \mathbf{y}_2^-, t)$, $\mathbf{g}_{12} = \mathbf{v}_{\mathrm{p}2} - \mathbf{v}_{\mathrm{p}1}$ and $\mathbf{n}_{12}$ has been defined above. The inequality $\mathbf{g}_{12}\cdot\mathbf{n}_{12} \leq 0$ is the condition of physical feasibility of a collision between the 1-st and the 2-nd particles, and the angles χ_{12} and ε_{12} specify the direction of $\mathbf{n}_{12}$ in spherical coordinates with the origin at the centre of the 1-st particle [26].

The function J which enters into the collisional integral depends on the particle-particle collision model which will be discussed later.

Let $\Phi = \Phi(\mathbf{x}_i)$ be a parameter of an individual particle. If a hydrodynamic parameter of a "gas" of particles (in other words, macroparameter of the dispersed phase) $\langle\Phi\rangle(\mathbf{r},t)$ at a point $\mathbf{r}$ of the physical space is defined as the ensemble averaged value of $\Phi = \Phi(\mathbf{x}_i)$ in a unit volume of the gas–particle mixture, then $\langle\Phi\rangle(\mathbf{r},t)$ can be expressed in terms of Φ and $f(\mathbf{x}_1,t)$ as follows:

$$\langle\Phi\rangle(\mathbf{r},t) = \int \Phi(\mathbf{r},\mathbf{y}_1,t) f(\mathbf{r},\mathbf{y}_1,t)\, d\mathbf{y}_1. \tag{12}$$

For example, the particle numerical density n_p, the particle volume fraction α_p, the hydrodynamic velocity $\mathbf{w}_\mathrm{p}$ and the specific energy of the particle chaotic motion e_p are calculated as follows:

$$n_\mathrm{p} = \langle 1\rangle, \quad \alpha_\mathrm{p} = \frac{4}{3}\pi r_\mathrm{p}^3 n_\mathrm{p}, \quad \mathbf{w}_\mathrm{p} = \frac{\langle \mathbf{v}_\mathrm{p}\rangle}{n_\mathrm{p}}, \quad e_\mathrm{p} = \frac{1}{m_\mathrm{p} n_\mathrm{p}} \left\langle \frac{m_\mathrm{p}(\mathbf{v}_\mathrm{p} - \mathbf{w}_\mathrm{p})^2}{2} \right\rangle.$$

A model of a non-completely elastic collision between two particles is an important part of the kinetic model. The momentum and angular momentum balance equations for a pair of i-th and j-th colliding spherical particles can be written in the form:

$$m_\mathrm{p}\mathbf{v}_{\mathrm{p}i}^- + m_\mathrm{p}\mathbf{v}_{\mathrm{p}j}^- = m_\mathrm{p}\mathbf{v}_{\mathrm{p}i}^+ + m_\mathrm{p}\mathbf{v}_{\mathrm{p}j}^+, \qquad I_\mathrm{p}(\mathbf{\Omega}_{\mathrm{p}k}^+ - \mathbf{\Omega}_{\mathrm{p}k}^-) = m_\mathrm{p} r_\mathrm{p} \mathbf{e}_k \times (\mathbf{v}_{\mathrm{p}k}^+ - \mathbf{v}_{\mathrm{p}k}^-), \qquad k = i, j, \tag{13}$$

where $\mathbf{e}_i = \mathbf{n}_{ij}$, $\mathbf{e}_j = -\mathbf{n}_{ij}$. The system of these three equations is not closed because it involves four unknowns $\mathbf{v}_{\mathrm{p}k}^+$ and $\mathbf{\Omega}_{\mathrm{p}k}^+$, $k = i, j$. Some additional hypotheses for the interaction between particles should be introduced to make this system closed. Considering the relative velocity of particles at the contact point

$$\mathbf{U}_{ij} = \mathbf{v}_{\mathrm{p}j} - \mathbf{v}_{\mathrm{p}i} - r_\mathrm{p}(\mathbf{\Omega}_{\mathrm{p}i} + \mathbf{\Omega}_{\mathrm{p}j}) \times \mathbf{n}_{ij} \tag{14}$$

we represent $\mathbf{U}_{ij}^+$ in the form

$$\mathbf{U}_{ij}^+ = -a_{\mathrm{p}n}\mathbf{U}_{ij(n)}^- + a_{\mathrm{p}t}\mathbf{U}_{ij(t)}^-, \tag{15}$$

where $a_{\mathrm{p}n}$ and $a_{\mathrm{p}t}$ are the restitution coefficients of the normal ($\mathbf{U}_{ij(n)} = (\mathbf{U}_{ij}\cdot\mathbf{n}_{ij})\mathbf{n}_{ij}$) and tangential ($\mathbf{U}_{ij(t)} = \mathbf{U}_{ij} - \mathbf{U}_{ij(n)}$) components of the relative velocity $\mathbf{U}_{ij}$. These coefficients are assumed to take into account the loss of the particles' kinetic energy due to inelastic collisions ($a_{\mathrm{p}n}$) and due to the particles' surface friction ($a_{\mathrm{p}t}$). Their values lie in the ranges: $0 \le a_{\mathrm{p}n} \le 1$, $-1 \le a_{\mathrm{p}t} \le 1$.
The true values of $a_{\mathrm{p}n}$ and $a_{\mathrm{p}t}$ in different conditions of a collision are unknown. We assume these restitution coefficients to be constant. If the values of $a_{\mathrm{p}n}$ and $a_{\mathrm{p}t}$ are given, then the system of equations becomes closed and can be solved for the parameters of i-th and j-th particles after their collision. In this case we can also calculate the Jacobian $J_1 = |D(\mathbf{y}_i^+, \mathbf{y}_j^+)/D(\mathbf{y}_i^-, \mathbf{y}_j^-)| = -a_{\mathrm{p}n}a_{\mathrm{p}t}^2$ and then the parameter J in the collisional integral: $J = a_{\mathrm{p}n}^2 a_{\mathrm{p}t}^2$. In reality, the absolute values of $a_{\mathrm{p}n}$ and $a_{\mathrm{p}t}$ are always less than a unity, hence $J < 1$. The multiplier $1/J$ in the collisional integral takes into account the "compression" of the phase space caused by the losses of the kinetic energy of colliding particles.

6. Model of the carrier gas flow

In the present study the particle volume fraction is assumed to be low enough so that the reverse effect of the particle phase on the carrier gas is negligible. We consider two-dimensional supersonic dusty gas flow over a cross-wise cylinder at not too high Reynolds number so that the flow is laminar. In this case the flow can be described by the Navier–Stokes equations, which can be written in Cartesian coordinates (x, y) in the following compact form [33]:

$$\frac{\partial \mathbf{Q}}{\partial t} + \frac{\partial \mathbf{F}_x}{\partial x} + \frac{\partial \mathbf{F}_y}{\partial y} = \frac{\partial \mathbf{G}_x}{\partial x} + \frac{\partial \mathbf{G}_y}{\partial y}, \tag{16}$$

where the vectors $\mathbf{Q}$, $\mathbf{F}_x$, $\mathbf{F}_y$, $\mathbf{G}_x$ and $\mathbf{G}_y$ are defined as follows

$$\mathbf{Q} = \begin{pmatrix} \rho \\ \rho u \\ \rho v \\ \rho e \end{pmatrix}, \quad \mathbf{F}_x = \begin{pmatrix} \rho u \\ \rho u^2 + p \\ \rho uv \\ (\rho e + p)u \end{pmatrix}, \quad \mathbf{F}_y = \begin{pmatrix} \rho v \\ \rho uv \\ \rho v^2 + p \\ (\rho e + p)v \end{pmatrix}, \tag{17}$$

$$\mathbf{G}_x = \begin{pmatrix} 0 \\ \tau_{xx} \\ \tau_{xy} \\ u\tau_{xx} + v\tau_{xy} - q_x \end{pmatrix}, \quad \mathbf{G}_y = \begin{pmatrix} 0 \\ \tau_{xy} \\ \tau_{yy} \\ u\tau_{xy} + v\tau_{yy} - q_y \end{pmatrix}.$$

Here,

$$\tau_{xx} = \frac{2}{3}\mu\left(2\frac{\partial u}{\partial x} - \frac{\partial v}{\partial y}\right), \quad \tau_{yy} = \frac{2}{3}\mu\left(2\frac{\partial v}{\partial y} - \frac{\partial u}{\partial x}\right), \quad \tau_{xy} = \mu\left(\frac{\partial u}{\partial y} + \frac{\partial v}{\partial x}\right), \tag{18}$$

$$q_x = -\lambda\frac{\partial T}{\partial x}, \quad q_y = -\lambda\frac{\partial T}{\partial y}, \quad p = \rho RT, \quad e = c_v T + \frac{u^2+v^2}{2}. \tag{19}$$

In these equations, t is the time; (xy) is the plane of flow, u and v are the x- and y-components of the velocity vector; ρ, p, e, T, μ and λ are the gas density, pressure, specific total energy, temperature, viscosity, and thermal conductivity, respectively; R is the gas constant; and c_V is the specific heat at constant volume. For μ and λ the following relations were used $\mu = \mu_s(T/T_s)^{3/2}(T_s + C_s)/(T + C_s)$ and $\lambda = c_p\mu/\mathrm{Pr}$, where the first relation is the Sutherlend formula (for the air $\mu_s = 1.71 \cdot 10^{-5}$ N·s/m^2, $T_s = 288$ K, $C_s = 117$ K); Pr is the Prandtl number; and c_p is the specific heat at constant pressure. The above system of equations is closed.

7. Gas-particle flow over a cylinder: results and discussion

At first, the equations 16–19 were solved numerically by CFD method with high accuracy. Total number of grid cells in the shock layer was about 250 thousands. A number of cells along the cylinder contour from the stagnation point to the maximal cross-section was one thousand, and across the boundary layer about 15. Steady-state flow was obtained as a limit of unsteady solution at large time. Input data for computational simulation were taken as follows: the cylinder diameter $D = 20$ mm, the free stream velocity $V_\infty = 600$ m/s, the pressure $p_\infty = 853$ Pa, the temperature $T_\infty = 88.7$ K. These values correspond to the Mach number $\mathrm{M}_\infty = 3.18$ and the Reynolds number $\mathrm{Re} = \rho_\infty \mathrm{V}_\infty \mathrm{D}/\mu_\infty = 0.7 \cdot 10^5$. The Prandtl number was equal to $\mathrm{Pr} = 0.71$. At the cylinder surface the normal and tangential velocity components were zero, the temperature was $T_w = 300$ K.

Motion and interaction of a particle cloud with the cylinder was studied to investigate the effects of scattering of rebounded non-spherical particles, the particle-particle collisions and the particle size distribution in formation of the particle phase flow structure. The model of the particle-wall collision described in Section 2 was used. Computational simulation of "collisional gas" of particles in the carrier gas flow was performed by the Direct Simulation Monte Carlo (DSMC) method described in detail in [34]. In calculations, the restitution coefficients for colliding particles entering the relation 15 were taken as follows: $a_{\mathrm{p}n} = 0.5$ and $a_{\mathrm{p}t} = 0.9$. The initial position and configuration of a cloud ($L = 100$ mm, $B = 20$ mm) is shown in Fig. 8.

Particles in an undisturbed flow were assumed to have the velocity and the temperature equal to those of the carrier gas. The carrier gas flow was considered as two-dimensional, but the motion of every particle was simulated as three-dimensional. The particle material density was equal to $\rho_{\mathrm{p}}^\circ = 2650$ kg/m^3. The size of spherical particles was equal to their diameter d_{p}. For non-spherical particles, the size was equal to the dimension in ξ-direction (see Fig. 2). In calculations the particle size was varied from 1 μm to 10 μm. These particle parameters together with the parameters taken for the gas flow correspond to the Stokes number $\mathrm{Stk} = \rho_{\mathrm{p}}^\circ d_{\mathrm{p}}^2 V_\infty/(18\mu_\infty D)$ from 0.77 (particles of medium inertia) to 77 (coarse particles of high inertia). The results are given in Figs. 9–12.

Instant patterns of coarse spherical and non-spherical prismatic particles rebounded from the forward part of a cylinder are shown in Fig. 9. For low particle concentration when collisions between particles are negligible (see top row of pictures), a particle shape have a pronounced effect on the particle phase flow structure. The strongest effect is observed for prismatic particles and prismatic particles with cut vertices. These prismatic particles fly off from the cylinder surface after rebound much farther than spherical and ellipsoidal ones of the same size. Such difference in behaviour of, say,

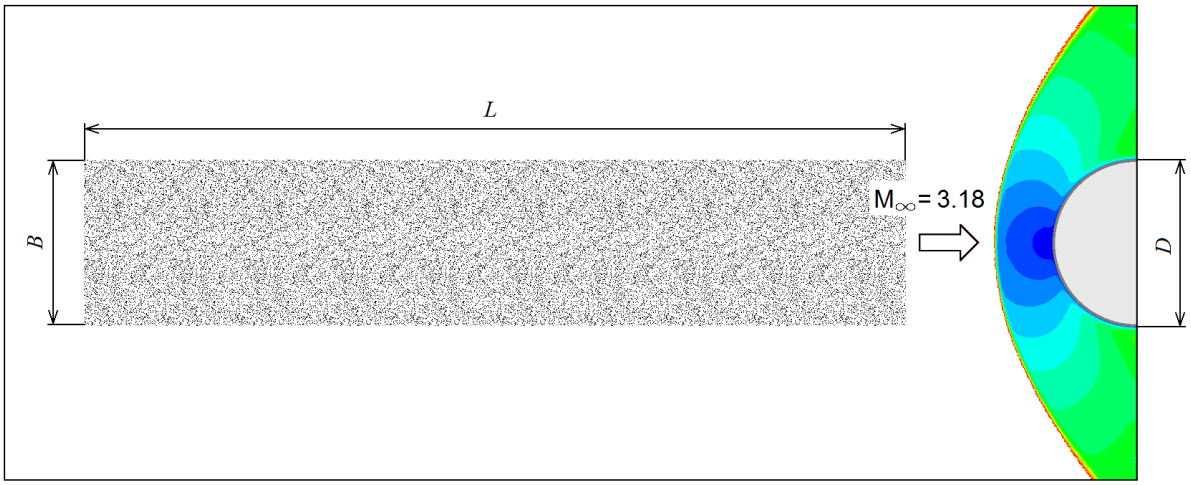

Figure 8 – Initial configuration of a particle cloud in an undisturbed flow.

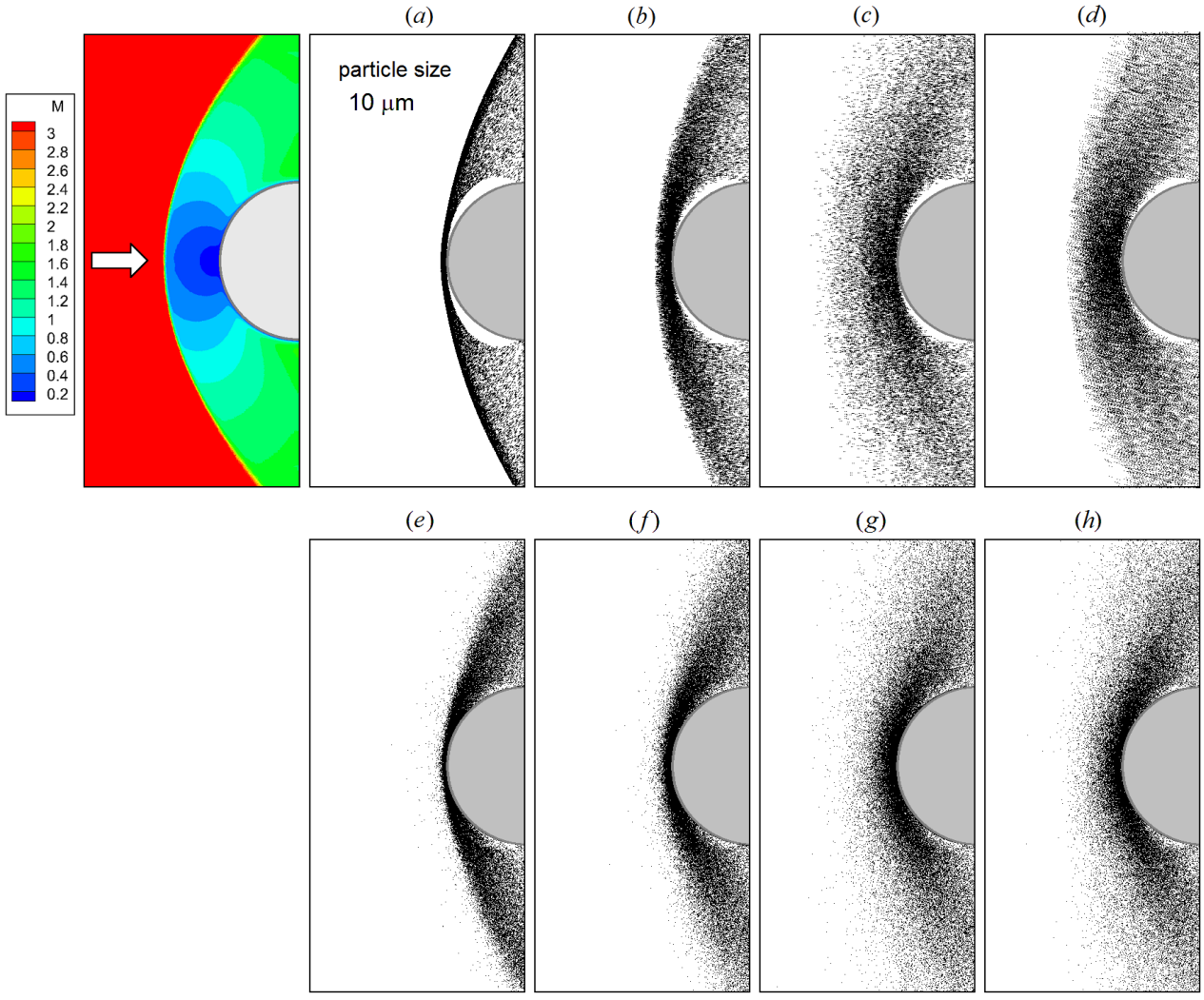

Figure 9 – Field of Mach number in the carrier gas and instant patterns of monosized (10 μm) rebounded particles of different shape with fixed parameters: spherical particles (*a*), (*e*), prolate ellipsoids with $b/a = c/a = 0.8$ (*b*), (*f*), prismatic particles with cut vertices with $b/a = c/a = 0.8$ (*c*), (*g*), and prismatic particles with $b/a = c/a = 0.8$ (*d*), (*h*); particle-particle collisions are not taken into account (*a*)–(*d*); particle-particle collisions are taken into account (*e*)–(*h*).

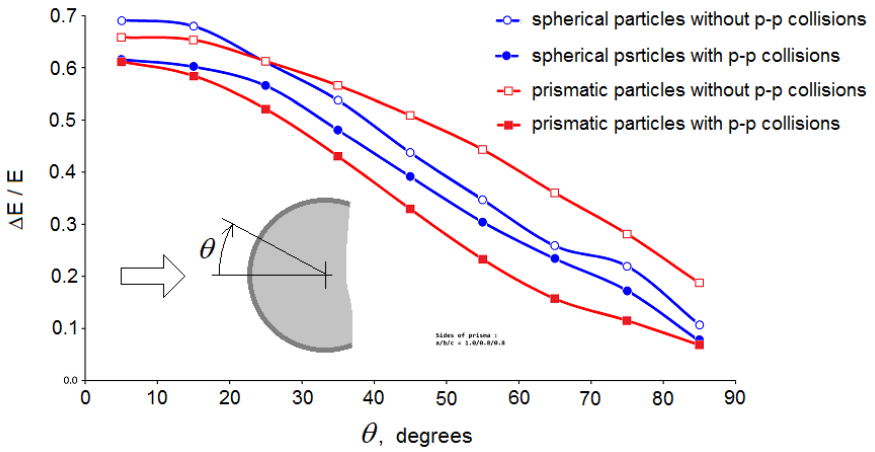

Figure 10 – Effect of the particle shape and the particle-particle (p-p) collisions on the particle kinetic energy loss during particle phase interaction with the forward part of a cylinder. $\alpha_{p\infty} = 10^{-3}$.

spherical and prismatic particles can be explained by that the value of the most probable normal velocity of rebounded prismatic particle is much higher (two times higher at the impact angle of 90°) than for spherical particles (see Fig. 5). In Fig. 9 the results for "collisional gas" of particles are also displayed (see bottom row of pictures). As is seen the particle-particle collisions can distinctly affect the particle phase flow pattern even at rather low particle concentration (the particle volume fraction in an undisturbed flow was equal to $\alpha_{p\infty} = 10^{-3}$). Note that at $\alpha_{p\infty} = 10^{-4}$ collisions between particles play no role.

The layer of chaotically moving and colliding with each other particles near the forward part of a cylinder has a shielding effect on high-speed particles from an undisturbed flow. These particles cannot reach the cylinder surface with high speed because they interact with this layer through collisions with chaotically moving particles and lose their speed. The quantitative shielding effect is demonstrated by Fig. 10 where the relative kinetic particle lost $\Delta E/E$ during the particle cloud interaction with a cylinder versus the angle θ (shown in Figure) is displayed for two particle shapes. For every particle the energy lost $\Delta E_p/E_p$ is defined by relations

$$\Delta E_p = \frac{1}{2}[m_p(v_p^-)^2 + J_p(\omega_p^-)^2] - \frac{1}{2}[m_p(v_p^+)^2 + J_p(\omega_p^+)2], \qquad E_p = \frac{1}{2}m_p v_{p\infty}^2.$$

It is clearly seen that for both, spherical and prismatic, particles this effect is pronounced (for prismatic particles it expressed stronger). Note that prismatic particles experience as a rule from 2 to 5 collisions during one rebound, and they much stronger twisted in particle-wall collisions that spherical ones.

The particle energy loss is distributed between rebounded particles, cylinder, and the carrier gas, however this distribution is unknown and requires further experimental and theoretical investigations. This question is of great importance for prediction of the body erosion rate in a gas-particle flow.

Next point in the present study is the effect of particle size dispersion. As is known, real particles never have the same size. For the particle distribution in size in a initial particle cloud we took the lognormal law:

$$g_\infty(d_p) = \frac{1}{\sqrt{2\pi}\, d_p \log\sigma} \exp\left[-\left(\frac{\log d_p - \log d_g}{\sqrt{2}\log\sigma}\right)^2\right] \tag{20}$$

where parameter d_g is related with the most probable particle size d_{pm} by the formula $d_g = d_{pm}\exp(\log^2\sigma)$. Calculations were performed for σ = 1.2 and 1.728. Plots of g_∞ are shown in Fig. 11.

In Fig. 12 are given the particle phase flow patterns for monosized and polydispersed prismatic particles. It is seen that the effect of the particle size dispersion is expressed very weakly, much weaker than the effects of particle shape and particle-particle collisions.

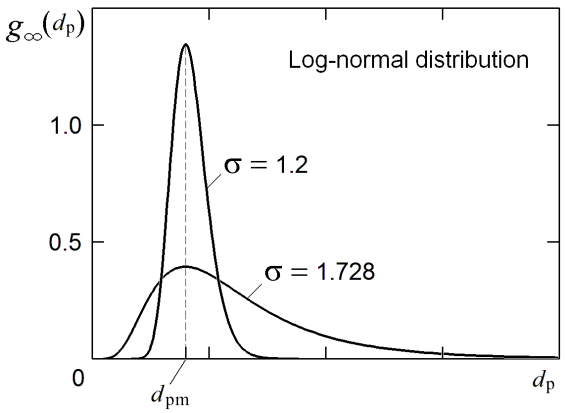

Figure 11 – Lognormal law of particle size distribution in an initial cloud.

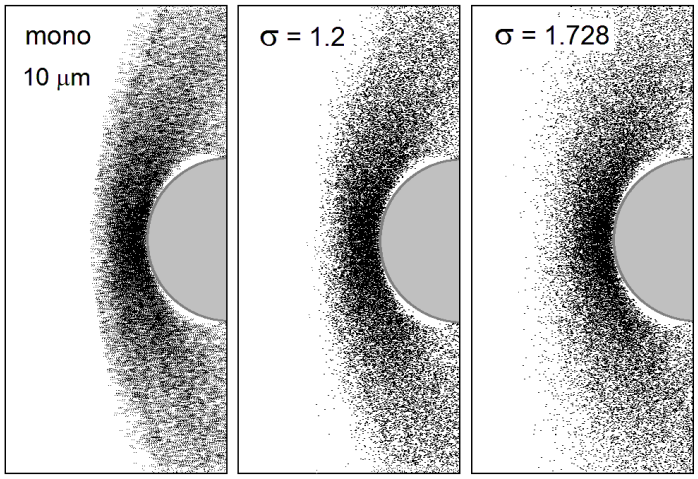

Figure 12 – The effect of particle size dipersion on the particle phase flow pattern.

8. Conclusion

Computational simulation of supersonic two-phase gas-particle flow over a blunt body (cylinder) was performed with taking account for the following effects of random nature: scattering of particles rebounded from the body surface due to non-spherical particle shape, collisions between particles, and particle size dispersion. Several non-spherical particle shapes were considered: ellipsoids, rectangular parallelepiped (prismatic particles) and rectangular parallelepiped with cut vertices, and the results were compared with those for spherical particles. Calculations were performed for medium to highly inertial particles (Stokes number was varied from a value of order of a unity to several tens). The most important conclusions are sum up below.

It was found that rebounding of non-spherical particles is accompanied very often by two and more particle-wall collisions. Such particles are strongly twisted, and the magnitude of their normal velocity after a rebound is much higher than that for spherical particles. Non-spherical particles fly away from the forward part of a blunt body much farther than spherical ones of the same size.

All considered random phenomena (scattering of rebounded particles, particle-particle collisions and particle size distribution) have different effects on the particle phase flow pattern. The effect of scattering is of primary importance for any particle concentration. Collisions between particles begin to play a noticeable role for rather high particle concentration, when the particle mass load in the flow is close to that for the carrier gas. For considered two-phase flow parameters, the particle size dispersion has a weak effect even for rather high dispersion in an undisturbed flow.

The particle shape and the particle-particle collisions has a essential effect on the particle kinetic energy loss during rebounding. Collisions between particles result in formation of a rather dense layer of chaotically moving particles near the body surface. This layer inhibits high-speed particles impacts on the body surface producing a shielding effect.

The present study has shown that all considered effects can play an important role in gas-particle flows over bodies, and they should be taken into account.

9. Acknowledgements

The present study was supported by the Russian Foundation for Basic Research (grant 20-08-00711).

10. Contact Author Email Address

mailto: Yury-Tsirkunov@rambler.ru

11. Copyright Statement

References

[1] Mikhatulin D.S., Polezhaev Yu.V. and Reviznikov, D.L. *Heat Transfer and Destruction of Bodies in Supersonic Heterogeneous Flow*. Yanus-K, Moscow, 2007. [in Russian]

[2] Tsirkunov Yu.M. Gas-particle flows around bodies – key problems, modeling and numerical analysis. *Proc. 4th Int. Conf. on Multiphase Flow: CD-ROM Proceedings ICMF'2001*, May 27-June 1, 2001, New Orleans, LA, USA. Ed.: E. Michaelides. Paper No. 607, pp. 1–31. 2001.

[3] Vasilevskii E.B., Osiptsov A.N., Chirikhin A.V. and Yakovleva L.V. Heat exchange on the front surface of a blunt body in a high-speed flow containing low-inertia particles. *Journal of Engineering Physics and Thermophysics*, Vol. 74, No. 6, pp. 1399–1411, 2011.

[4] Golubkina I.V., Osiptsov A.N. and Sakharov V.I. Supersonic low-concentration dusty-gas flow past a plane cylinder in the presence of an oblique shock wave interacting with the bow shock. *Fluid Dynamics,*, Vol. 46, No. 1, pp. 51–63, 2011.

[5] Oesterle B., Volkov A.N. and Tsirkunov Yu.M. Numerical investigation of two-phase flow structure and heat transfer in a supersonic dusty gas flow over a blunt body. *Progress in propulsion physics. Vol. 5*, TORUS PRESS / EDP Sciences, pp. 441–456, 2013.

[6] Majid A., Bauder U., Herdrich G. and Fertig M. Two-phase flow solver for hypersonic entry flows in a dusty Martian atmosphere. *Journal of Thermophysics and Heat Transfer*, Vol. 30, No. 2, pp. 418–428, 2016.

[7] Reviznikov D.L., Sposobin A.V. and Ivanov I.E. A change in the structure of a flow under the action of highly inertial particle when a hypersonic heterogeneous flow passes over a body. *High Temperature*, Vol. 56, No. 6, pp. 884–889, 2018.

[8] Varaksin A.Yu. Gas-solid flows past bodies. *High Temperature*, Vol. 56, No. 2, pp. 275–295, 2018.

[9] Haider A. and Levenspiel O. Drag coefficient and terminal velocity of spherical and nonspherical particles. *Powder Technology*, Vol. 58, No. 1, pp. 63–70, 1989.

[10] Hölzer A. and Sommerfeld M. New simple correlation formula for the drag coefficient of non-spherical particles. *Powder Technology*, Vol. 184, pp 361–365, 2008.

[11] Hölzer A. and Sommerfeld M. Lattice Boltzmann simulations to determine drag, lift and torque acting on non-spherical particles. *Computers & Fluids* , Vol. 38, pp. 572–589, 2009.

[12] Amelyushkin, I.A. and Stasenko, A.L. Interaction of a gas flow carrying nonspherical microparticles with a cross cylinder. *Journal of Engineering Physics and Thermophysics*, Vol. 91, No. 2, pp. 288–299, 2018.

[13] Sommerfeld M. Kinetic simulation for analysing the wall collision process of nonspherical particles. *Proc. of ASME FEDSM'2002*, July 14-18, 2002, Montreal, Quebec, Canada, paper No. 31239, pp. 1–10, 2002.

[14] Panfilov S.V. and Tsirkunov Yu.M. Scattering of nonspherical particles rebounding from a smooth and a rough surface in a high-speed gas-particle flow. *J. Appl. Mech. Tech. Phys.*, Vol. 49, No. 2, pp. 222–230, 2008.

[15] Arboleda B.Q., Qadir Z., Sommerfeld M. and Beatove S.L. Modelling the wall collision of regular non-spherical particles and experimental validation. *ASME FEDSM'2014 Proceedings*, Paper No. 21610, pp. 1–12, 2014.

[16] Quintero B., Lain S. and Sommerfeld M. Derivation and validation of a hard-body particle-wall collision model for non-spherical particles of arbitrary shape. *Powder Technology*, Vol. 380, pp. 526–538, 2021.

[17] Tsirkunov Yu.M., Romanyuk D.A. and Panfilov S.V. Effects of particle mixing and scattering in the dusty gas flow through moving and stationary cascades of airfoils. *Progress in Propulsion Physics, Vol. 2*. EDP Sciences, pp. 459–474. 2011.

[18] Reviznikov D.L., Sposobin A.V. and Sukharev T.Yu. Numerical simulation of the flow around a blunt body in supersonic polydisperse stream. *High Temperature*, Vol. 55, No. 3, pp. 400–406, 2017.

[19] Tabakoff W., Malak M.F. and Hamed A. Laser measurements of solid-particle rebound parameters impacting on 2024 aluminium and 6A1-4V titanium alloys. *AIAA Journal*, Vol. 25, No. 5, pp. 721–726, 1987.

[20] Lashkov V. A. Experimental determination of the coefficients of restitution of particles in the flow of a gas suspension in a collision against the surface. *J. Eng. Phys. Thermophys.*, Vol. 60, No. 2, pp. 154–159, 1991.

[21] Sommerfeld H., Koch Ch., Schwarz A. and Beck A. High velocity measurements of particle rebound characteristics under erosive conditions of high pressure compressors, *Wear*, pp. 470–471, 203626, 2021.

[22] Stasenko A.L. Velocity recovery factors of a particle repelled from a solid surface. *J. Eng Phys. Thermophys.*, Vol. 80, No. 5, pp. 885–891, 2007.

[23] Lashkov V.A. Coefficient of restitution under normal impact. *Bull. of St. Petersburg. Univ. Ser. 1*, No. 4, pp. 127–136. [in Russian].

[24] Singh S. and Tafti D. Predicting the coefficient of restitution for particle wall collisions in gas turbine components. *Proc. of ASME Turbo Expo 2013*, June 3–7, 2013, San Antonio, Texas, USA, paper GT2013-95623, pp. 1–9, 2013.

[25] Ray S., Kempe T., Frölich J. Efficient modelling of particle collisions using a nonlinear viscoelastic contact force. *International Journal of Multiphase Flow*, Vol. 76, pp. 101–110, 2015

[26] Volkov A.N. and Tsirkunov Yu.M. Kinetic model of a collisional admixture in dusty gas and its application to calculating flow past bodies. *Fluid Dynamics.* Vol. 35, No. 3, pp. 380–392, 2000.

[27] Tsirkunov Yu.M., Panfilov S.V. and Klychnikov M.B. Semiempirical model of impact interaction of a disperse impurity particle with a surface in a gas suspension flow. *J. Engng. Phys. Thermophys*. Vol. 67, No. 5-6, pp. 1018–1025, 1994.

[28] Crowe C.T., Schwarzkopf J.D., Sommerfeld M. and Tsuji Y. *Multiphase Flows with Droplets and Particles*. 2nd Edition, CRC Press, Boca Raton, USA, 2012.

[29] Henderson Ch.B. Drag coeccients of spheres in continuum and rarefied flows. *AIAA Journal*, Vol. 14, No. 6, pp. 707–708, 1976.

[30] Rubinow S.I. and Keller J.B. The transverse force on a spinning sphere moving in a viscous fluid. *J. Fluid Mech.*, Vol. 11, pp. 447–459, 1961.

[31] Oesterlé B. and Bui Dinh T. Experiments on the lift of a spinning sphere in a range of intermediate Reynolds numbers. *Experim. in Fluids*, Vol. 25, pp. 16–22, 1998.

[32] Dennis S.C.R., Singh S.N. and Ingham D.B. The steady flow due to a rotating sphere at low and moderate Reynolds numbers. *J. Fluid Mech.*, Vol. 101, pp. 257–279, 1980.

[33] Anderson D.A., Tannehill J.C. and Pletcher R.H. *Computational Fluid Mechnics and Heat Transfer*. Hemisphere Publ. Corp., New York, 1984.

[34] Volkov A.N. and Tsirkunov Yu.M. CFD/Monte Carlo simulation of collision-dominated gas-particle flows over bodies. *Proc. of ASME FEDSM'2002*, July 14-18, 2002, Montreal, Quebec, Canada, paper No. 31222, pp. 1–14, 2002.